Preprints (www.preprints.org) | NOT PEER-REVIEWED | Posted: 25 October 2018 doi:10.20944/preprints201810.0609.v1

Article

The Concept of Comprehensive Data Analysis from Ultra-Wideband Subsystem for Smart City Positioning Purposes

Damian Grzechca *, Krzysztof Hanzel and Krzysztof Paszek

Faculty of Automatic Control, Electronics and Computer Science,
Silesian University of Technology Gliwice, Poland; Krzysztof.Hanzel@polsl.pl; Krzysztof.Paszek@polsl.pl
* Correspondence: Damian.Grzechca@polsl.pl; Tel.: +48-32-237-2717

Abstract: As a part of the proposed article, the authors presented comprehensive data analysis for movement data that comes from a positioning system based on ultra-wide band (UWB) technology. For purpose of this article, a test was carried out during which the car equipped with cruise control overcame the given path at a speed from 10 km/h to 60 km/h. The obtained motion models (information about position) have been filtered through a series of filters - from fundamentals filters with a variable window (median, moving average, Savitzky-Golay filter), through more complex ones like the Wiener or Kalman filter. As a result, the authors proposed a form of data analysis and filtration depending on the speed of the moving object. In addition, the maximum accuracy that can be obtained for a given traffic model was also determined. The whole research proves that it is possible to use a system based on UWB technology in positioning objects for urban applications - smart city, in industry 4.0 applications as well as for positioning autonomous vehicles in urban applications, such as well as on highways to maintain cohesion of convoys vehicles.

Keywords: positioning; ultra-wide band; filtration; Kalman filter; smart city; industry 4.0

1. Introduction

Determining the position of objects is now a very important function of many applications in the field of industry and urban solutions. In the implementation of this issue, many technologies are used, and several divisions can be specified, for example on Indoor Positioning Systems (IPS) or Outdoor Positioning Systems (OPS) [1]. Some of the technologies seem to be closely related to a specific application – for example, the use of global positioning system (GPS) in OPS applications [2–4]) or positioning using Radio-frequency Identification (RFID) tags in IPS applications [5,6]). There are technologies that, due to their accuracy, play an assisting role (e.g. Microelectromechanical systems (MEMS) [7], Wi-Fi [8–10] or GSM [11] as GPS assist systems). Finally, there are attempts to use various other systems for the role of localization systems such as Bluetooth [12–15], Zigbee [16,17], Infrared [18], Vision systems [19–21] etc.. As you can see, most of the available systems are implemented in IPS, and their use outside closed spaces meets with many limitations, such as operating range (Bluetooth, Zigbee, Infrared), stability (MEMS) or required technical facilities (vision systems).

An ever-growing society needs precise location, especially in heavily urbanized urban spaces, where the GPS signal is disturbed by buildings. Also, an industry seeks to maximize profits through the optimization and automation of production process. To meet these requirements they need a single, universal system that ensures a precise position in both IPS and OPS applications. Ultra-wideband (UWB) technology can be the answer to this demand – although it is already well known and described in the case of IPS applications [1,22,23] – it is still waiting to be discovered in outdoor applications.

As the UWB technology is the subject of many cross-cutting works [1], none of them has a description of how this technology works in the case of objects moving at high speed, the authors

© 2018 by the author(s). Distributed under a Creative Commons CC BY license.

Preprints (www.preprints.org) | NOT PEER-REVIEWED | Posted: 25 October 2018 doi:10.20944/preprints201810.0609.v1

decided to carry out research aimed at sensibility of using this technology in such applications. One of the additional impulses motivating the research was the fact that on the current level of development of this technology, automotive companies are already conducting research on optimal UWB placement of antennas on cars [24], which in the future is to apply to maintenance-free opening of vehicles. Manufacturers of UWB systems themselves perform accuracy tests based on speed, but they focus mainly on IPS applications. An example is a leading company producing UWB modules and their tests of DWM1000 modules, which showed accuracy of 10cm at speeds up to 5 m/s (18 km/h) [25]. Therefore, it has been intriguing whether it is possible to apply this technology in the positioning of moving vehicles, and with what efficiency we will have to deal with it.

In connection with the above, the authors carried out research to determine whether it is possible to use UWB technology for positioning vehicles moving at a regular, urban speed, and which path in data processing should be chosen so that the positioning accuracy is as high as possible. The effect of the authors' work was to become the answer whether the UWB is a technology that is a response to the demands that in the context of positioning puts such areas of life as smart city, autonomous vehicles or industry 4.0.

2. Materials and Methods

2.1. Data analysis process

The process of tag position determination was connecting few steps of data acquisition and signal processing. At the hardware level there were several ways to obtain distance from the time and propagation velocity of the electromagnetic wave [23]. In presented system the TDoA (time difference of arrival) was used (see Section 2.2).

Figure 1 presents flow data diagram which represent several steps in analysis of data that was obtained from hardware. The data frame F that was received from hardware included not only distances to particular nodes (D) but also timestamp, quality factor and receive signal strength indicator. So, in first step the information about distances had to be selected to further data analysis.

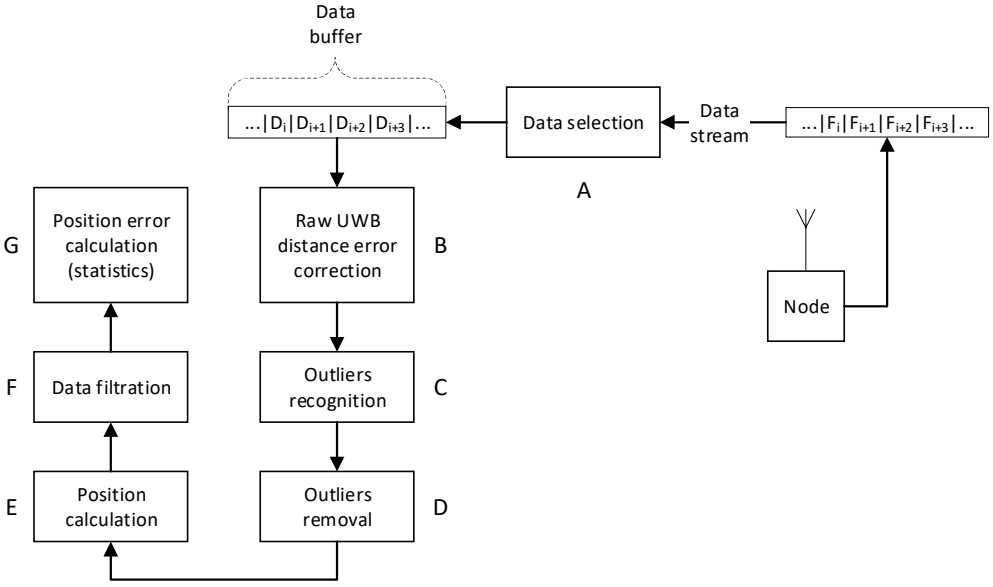

Figure 1. Data flow in the system – from hardware to accuracy calculation

Data buffer contained actually analysed distances from ranging system ($D_i = \{d_{A1}, d_{A2}, d_{A3}, d_{A4}\}$). In fact, it was the FIFO (first in firs out) queue with the size of used window width. Raw distances can be burdened with error that depends on distance between nodes. This type of error was reduced (block B) by using a distance-dependent function (shape of the function and its arguments were

Preprints (www.preprints.org) | NOT PEER-REVIEWED | Posted: 25 October 2018 doi:10.20944/preprints201810.0609.v1

adjusted in background phase). Raw data should be analysed with respect to random system error. Outliers – data that was distant from other observations in window, are detected (block C) by the use of: multiplied standard deviation; maximum difference between values in window according to velocity of the object; or combined of both previous (the value of this factor is signed ε). Found outliers can be corrected by the mean as well as median value (block D). After prefiltration processes position of the object was calculated (block E). Main data filtration (block F), like mean, median, Savitzky-Golay or Kalman and Wiener filters, was performed on object position in each axis separately. Statistical measures, like RMSE (root mean square error), were used to check if the filtration process gives improvement in position (block G).

2.2. Ranging algorithm and device

Particular distance between nodes was calculated by the use of travel time of a radio signal and the velocity of propagation of the electromagnetic wave. The communication process is presented in the Figure 2.

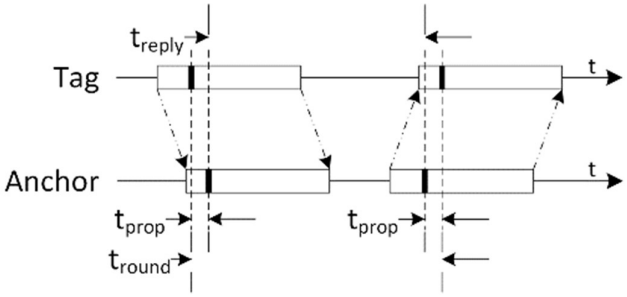

Figure 2. Communication between UWB Anchor and Tag

The obtained wave propagation time – t_{prop}, was converted to the distance between nodes – tag, and particular anchor. The time of flight can be calculated with the use of the (1). When the time of flight was calculated, the distance between tag and particular anchor could be calculated with the use of the (2).

$$t_{prop} = \frac{t_{round} - t_{reply}}{2} \tag{1}$$

$$d = c \cdot t_{prop} \tag{2}$$

where: d – the distance between nodes; c – the speed of electromagnetic wave propagation; and t_{prop} – the wave propagation time between nodes.

The test stand consisted of a UWB tag – a movable devices that processes signals and calculates distances, and four anchors – a stationary, reference points, presented in Figure 3. All of these devices were made of DWM1000 chips manufactured by DecaWave, compatible with IEEE802.15.4-2011 standard. According to the manufacturer declaration, the system was designed to create a real-time (RT) indoor positioning systems (IPS). It allows to localize objects with 10 cm accuracy, with the maximum moving speed up to 5 m/s (with subject to IPS). This technology also provides high-speed data transmission up to 6.8 Mb/s [25]. The system (localized object) returned distances in centimetres (using TDoA) between the tag and following anchors.

Preprints (www.preprints.org) | NOT PEER-REVIEWED | Posted: 25 October 2018 doi:10.20944/preprints201810.0609.v1

(a) (b)

Figure 3. Elements of the UWB localization system. On the (a) hardware of the node (DecaWave DWM1000 with STM32 Microcontroller), on the (b) anchor (hardware of node in the box)

The four anchors defined the coordinate system, and the entire test stand was presented as is showed in Figure 4. Reference points (anchors) were placed on the ground, on a square of 5 m, and a car was moved from right to left through centre of the designed square – a track of the object is marked on the Figure 4 with a dashed arrow.

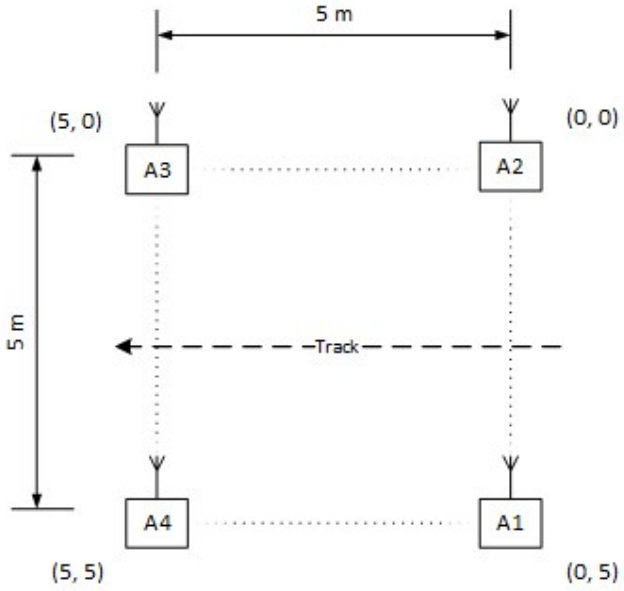

Figure 4. Diagram of the performed experiment – on the diagram the location of reference points [1-4], their coordinates (given in brackets) and the direction of vehicle travel were marked.

The experiment was performed for various speeds in the range from 2.78 m/s (10 km/h) up to 16.67 m/s (60km/h) every 2,78 m/s (10 km/h). The movement was carried out in a straight line, but it must be mentioned that the vehicle was driven by the human driver and the human factor influenced the exact trajectory. The UWB node – tag, was placed in the passenger side glove compartment, and two people in the front seats were in the car during the journey. Electronics devices like radio, chargers, mobile phones have been turned off in the car.

2.3. Data interpretation

As a result of the data acquisition in different test scenario, six measurement series (for difference speeds) were recorded – see Table 1.

Preprints (www.preprints.org) | NOT PEER-REVIEWED | Posted: 25 October 2018 doi:10.20944/preprints201810.0609.v1

Table 1. Speed of the object in different measuring series.

Series	Speed	
	[km/h]	[m/s]
R1	10	2.78
R2	20	5.56
R3	30	8.33
R4	40	11.11
R5	50	13.89
R6	60	16.67

Each series consisted of frames – F_i (for $i = 1 \dots N$) containing information about time, distances, RSSIs and quality indicator. The fields were as follow:

$$F_i = \{ts_i; D_i; RSSI_i; QI_i;\}$$

Fields description:

- N – total amount of data received from the UWB locating system;
- ts_i – time stamp (it is counted from the system start);
- $D_i = \{d_{A1}; d_{A2}; d_{A3}; d_{A4}\}$ – measured distances between tag and the following anchors (in cm);
- $RSSI_i = \{rssi_{A1}; rssi_{A2}; rssi_{A3}; rssi_{A4}\}$– signal strength indicator for the following anchors with respect to the Tag (in dBm);
- $QI_i = \{qi_{A1}; qi_{A2}; qi_{A3}; qi_{A4};\}$ – quality indicator for all anchors; no unit, values between 0 – the worst quality, and 1 – the best quality.

2.4. Position determination

The system (tag through the serial port – COM) returned distances D_i in centimetres between the tag and following anchors (as shown on datagram F_i). The trilateration algorithm was applied in order to convert the distances data to a position in created coordinate system.

The principle of operation flows from the fundamental geometry and the main idea is depicted in the Figure 5 [26]. There were three reference points (anchors) which were selected from all available, for example $A1$, $A2$ and $A3$. The position of the anchors were well known in three dimensions $A1 \rightarrow (x_1, y_1, z_1)$, $A2 \rightarrow (x_2, y_2, z_2)$, $A3 \rightarrow (x_3, y_3, z_3)$ as well as distance from tag to particular anchor d_{A1}, d_{A2} and d_{A3}.

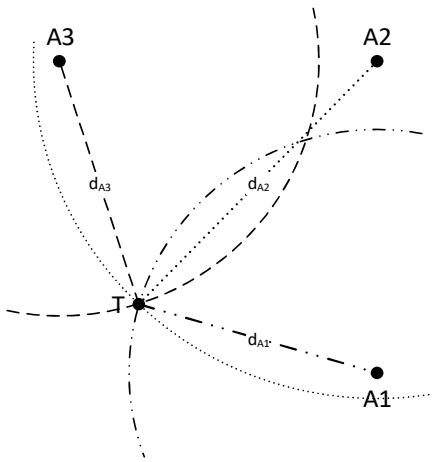

Figure 5. Trilateration – an example of the operation given for the point - the tag T, and for the three distances d_{A1}, d_{A2} and d_{A3} from the three reference points (anchors) $A1$, $A2$ and $A3$

Determining the coordinates of the localized point (tag) $T \rightarrow (x, y, z)$ is equivalent to the determination of the coordinates of the system of quadratic equations as is shown in (3).

Preprints (www.preprints.org) | NOT PEER-REVIEWED | Posted: 25 October 2018 doi:10.20944/preprints201810.0609.v1

$$\begin{cases}(x-x_1)^2+(y-y_1)^2+(z-z_1)^2=d_{A1}^2\\(x-x_2)^2+(y-y_2)^2+(z-z_2)^2=d_{A2}^2\\(x-x_3)^2+(y-y_3)^2+(z-z_3)^2=d_{A3}^2\end{cases} \quad (3)$$

Equation (3) can be arranged as (4)

$$\begin{cases}(x^2+y^2+z^2)-2x_1x-2y_1y-2z_1z=\ d_{A1}^2-x_1^2-y_1^2-z_1^2\\(x^2+y^2+z^2)-2x_2x-2y_2y-2z_2z=\ d_{A2}^2-x_2^2-y_2^2-z_2^2\\(x^2+y^2+z^2)-2x_3x-2y_3y-2z_3z=\ d_{A3}^2-x_3^2-y_3^2-z_3^2\end{cases} \quad (4)$$

or in matrix representation (5).

$$\begin{bmatrix}1 & -2x_1 & -2y_1 & -2z_1\\1 & -2x_2 & -2y_2 & -2z_2\\1 & -2x_3 & -2y_3 & -2z_3\end{bmatrix}\begin{bmatrix}x^2+y^2+z^2\\x\\y\\z\end{bmatrix}=\begin{bmatrix}d_{A1}^2-x_1^2-y_1^2-z_1^2\\d_{A2}^2-x_2^2-y_2^2-z_2^2\\d_{A3}^2-x_3^2-y_3^2-z_3^2\end{bmatrix} \quad (5)$$

Thus equation (5) is represented in the form (6), with the constraint (7).

$$\boldsymbol{A_0}\cdot\boldsymbol{x}=\boldsymbol{b_0} \quad (6)$$

$$x\in E$$
$$E=\{(x_0,x_1,x_2,x_3)^T\in\mathbb{R}^4\wedge x_0=x_1^2+x_2^2+x_3^2\} \quad (7)$$

In our case A_1, A_2 and A_3 did not lie on a straight line so the $rank(A_0)=3$ and $dim(Kern(A_0)=1$. The general solution of (6) is as equation (8).

$$\boldsymbol{x}=\boldsymbol{x}_p+t\cdot\boldsymbol{x}_h \quad (8)$$

where t is the real parameter, x_p is a particular solution of equation (8) and x_h is a solution of homogeneous system of equations (9) – a Basis of Kernel (A_0).

$$\boldsymbol{A_0}\cdot\boldsymbol{x}=0 \quad (9)$$

The x_p and x_h vectors can be determined using the Gaussian elimination method. The particular solution x_p can also be excluded by the pseudo inverse of the matrix A_0.

To determine the parameter t let do (10).

$$\begin{gathered}\boldsymbol{x_p}=(x_{p0},x_{p1},x_{p2},x_{p3})^T\\\boldsymbol{x_h}=(x_{h0},x_{h1},x_{h2},x_{h3})^T\\\boldsymbol{x}=(x_0,x_1,x_2,x_3)^T\end{gathered} \quad (10)$$

After inserted equations (10) through (8), the equation (11) is obtained.

$$\begin{cases}x_0=x_{p0}+t\cdot x_{h0}\\x_1=x_{p1}+t\cdot x_{h1}\\x_2=x_{p2}+t\cdot x_{h2}\\x_3=x_{p3}+t\cdot x_{h3}\end{cases} \quad (11)$$

After application of the constraint $x\in E$ it follows (12)

$$x_{p0}+t\cdot x_{h0}=\left(x_{p1}+t\cdot x_{h1}\right)^2+\left(x_{p2}+t\cdot x_{h2}\right)^2+\left(x_{p3}+t\cdot x_{h3}\right)^2 \quad (12)$$

and thus (13).

$$t^2(x_{h1}^2+x_{h2}^2+x_{h3}^2)+\ t\left(2x_{p1}x_{h1}+2x_{p2}x_{h2}+2x_{p3}h_{h3}-x_{h0}\right)+x_{p1}^2+x_{p2}^2+x_{p3}^2-x_{p0}=0 \quad (13)$$

This is a quadratic equation in the form $at^2+bt+c\ =\ 0$ with the solution as (14).

$$t_{1,2}=\frac{-b\pm\sqrt{b^2-4ac}}{2a} \quad (14)$$

The solutions of the equation system (8) are (15).

$$\begin{gathered}\boldsymbol{x_1}=\boldsymbol{x_p}+t_1\cdot\boldsymbol{x_h}\\\boldsymbol{x_2}=\boldsymbol{x_p}+t_2\cdot\boldsymbol{x_h}\end{gathered} \quad (15)$$

Preprints (www.preprints.org) | NOT PEER-REVIEWED | Posted: 25 October 2018 doi:10.20944/preprints201810.0609.v1

In the case of positioning using 3 anchors, the position of $T \rightarrow (x, y, z)$ can be represented as $x_1 \rightarrow (x, y, z)$ or $x_2 \rightarrow (x, y, z)$ depending on the expected range of positions in the X, Y and Z axes.

Applied multilateration algorithm does not require any additional range selection, because of the use of the additional reference point that allows us to indicate the point in three-dimensional space. However, it should be noted that in further considerations was made projection from the three-dimensional, to the two-dimensional view (by omitting the height data) from above of the road on which the object moved, due to the nature of the problem, and the lack of relevant data for traffic on the line, which could be obtained from the height information.

2.5. Outlier recognition and removal

As it was mentioned distances to particular anchor (generally after correction of distance related error) should be analysed to find random system error. Outliers in this system were detected (Figure 6) in window using mean value of distances without an i-th sample and the error factor ε which indicates the maximum value of the object shift (16).

$$\varepsilon = v \cdot \Delta t \cdot s \tag{16}$$

where: v – speed of the object; Δt – time difference; and s – scaling factor.

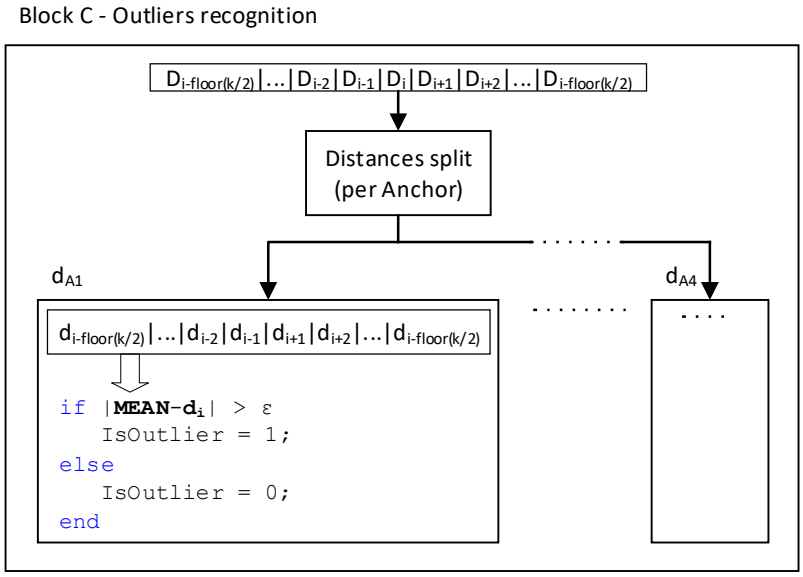

Figure 6. Outliers recognition process

When the outlier was recognized than the value of the distance could be replaced by the median or mean value in window.

2.6. Performed filtration

During the research different type of filtration methods have been applied to data after trilateration process with different widow size (3, 5, 9, 11, 13 and 15). Median filtration with window size k of x_i sample, where $i = 1, \ldots, k$ and $x_i \leq x_{i+1}$ is presented in equation (17).

$$med(x_i) = \begin{cases} x_{j+1} & for \quad k = 2j + 1 \\ \frac{1}{2}(x_j + x_{j+1}) & for \quad k = 2j \end{cases} \tag{17}$$

In this case, the k value was always an odd number, so the form for $k = 2_j + 1$ was used.

Another filtration method was moving average filter. This type of filtration reduces the amplitude of random outliers very well (18).

Preprints (www.preprints.org) | NOT PEER-REVIEWED | Posted: 25 October 2018 doi:10.20944/preprints201810.0609.v1

$$avg(x_i) = \frac{1}{\mathrm{k}} \sum_{\substack{j=-\lfloor \frac{k}{2} \rfloor \wedge \\ j \in \mathbb{Z}}}^{\lfloor \frac{k}{2} \rfloor} x_{i+j} \tag{18}$$

The next filtration method was Savitzky-Golay filter which is based on polynomial approximation by linear least squares method. This filter fit m degree polynomial to data in window so that the sum (ε_m) of squares of differences of values calculated from the approximating function (x'_{i+j}) and the value of the sample of the input signal (x_{i+j}) was as small as possible in the window (19).

$$\varepsilon_m = \sum_{j=-\lfloor \frac{k}{2} \rfloor}^{\lfloor \frac{k}{2} \rfloor} \left(x'_{i+j} - x_{i+j} \right)^2 \tag{19}$$

The new filtered value x' of x was calculated using approximated function coefficient c (20).

$$x'_{i+j} = \sum_{l=0}^{m} c_l (i+j)^l \tag{20}$$

Kalman filtering (KF), (also known as linear quadratic estimation – LQE), is an recursion algorithm that uses a series of measurements observed over time, containing statistical noise and other inaccuracies, and produces estimates of unknown variables that tend to be more accurate than those based on a single measurement alone [27,28].

The Kalman filter model assumes the true state at time (i) is evolved from the state at ($i-1$) (21).

$$\begin{aligned} x_i &= Ax_{i-1} + w_{i-1} \\ z_i &= Cx_{i-1} + v_{i-1} \end{aligned} \tag{21}$$

The classical form of a linear-discrete KF is given by prediction shown as (22),

$$\begin{aligned} &\hat{\boldsymbol{x}}(i|i-1) = A_i \hat{\boldsymbol{x}}(i-1|i-1) \\ &P(i|i-1) = A_i P(i-1|i-1) A_i^T + Q_{i-1} \\ &v_i = z_n - C\hat{\boldsymbol{x}}(i|i-1) \\ &S_i = C_i P(i|i-1) C_i^T + R \end{aligned} \tag{22}$$

and the filtering process in equations (23).

$$\begin{aligned} &K_k = P(i|i-1) C_i^T (S)^{-1} \\ &\hat{\boldsymbol{x}}(i|i) = \hat{\boldsymbol{x}}(i|i-1) + K_i v_i \\ &P(i|i) = (I_i - K_i C_i) P(i|i-1) \end{aligned} \tag{23}$$

Using the data properties which are characterized by the normal (Gaussian) distribution of samples, it was decided to use the Wiener filter. The Wiener filter [29] estimates local mean (24), and variance (25), around each sample

$$\mu = \frac{1}{MN} \sum_{n_1, n_2 \in \eta} x(n_1, n_2) \tag{24}$$

$$\sigma^2 = \frac{1}{MN} \sum_{n_1, n_2 \in \eta} x^2(n_1, n_2) - \mu^2 \tag{25}$$

where η is the M-by-N local neighborhood of sample x_i. Due to the fact that the filtered data are vector of the window width size (1-by-k) the above equation can be simplified as follow (26)(27).

$$\mu_i = \frac{1}{k} \sum_{j=-\lfloor \frac{k}{2} \rfloor}^{\lfloor \frac{k}{2} \rfloor} x_{i+j} \tag{26}$$

Preprints (www.preprints.org) | NOT PEER-REVIEWED | Posted: 25 October 2018 doi:10.20944/preprints201810.0609.v1

$$\sigma_i^2 = \frac{1}{k} \sum_{j=-\left\lfloor \frac{k}{2} \right\rfloor}^{\left\lfloor \frac{k}{2} \right\rfloor} x_{i+j}^2 - \mu_i^2 \tag{27}$$

The output of the filter is given by the formula (28),

$$x_i' = \mu_i + \frac{\sigma_i^2 - v^2}{\sigma_i^2}(x_i - \mu_i) \tag{28}$$

where v^2 is the variance of the noise.

The neighbourhood used in Wiener filtration is [5 1] which is equal to windows width of 5 samples.

2.7. Measure the value of the results

The results obtained were checked for several different statistical parameters. The first of these was the RMSE (root-mean-square error) (29).

$$RMSE_P = \sqrt{\frac{1}{N}\sum_{i=1}^{N}(x_i - \hat{x}_i)^2 + (y_i - \hat{y}_i)^2} \tag{29}$$

It allowed us to determine how much the distribution of points differs from the expected passage line for each of the measurement series.

The mean absolute error of position (MAE) from the estimated route was also considered (30).

$$MAE_P = \frac{1}{N}\sum_{i=1}^{N}\sqrt{(x_i - \hat{x}_i)^2 + (y_i - \hat{y}_i)^2} \tag{30}$$

This value allows you to determine how much the entire ride goes past the expected value.

Another value considered was the maximum deviation of the sample for each of the measurement series expressed by the formula (31)

$$MAX_P = \max_{i \in N}\left(\sqrt{(x_i - \hat{x}_i)^2 + (y_i - \hat{y}_i)^2}\right) \tag{31}$$

The value obtained from this metric allows us to determine how much carried out filtration affects the maximum error of samples from expected points, it means maximum error can be expected when moving along a straight line with the declared speed.

Each measurement series was different number of samples which were collected during the object movement. The reason is that the area of movement was limited and the different speed of the vehicle. To compare results of filtration method between different series – speeds (in fact different number of samples); the standard error (SE) was used.

$$SE_P = \frac{\sqrt{\frac{1}{N}\sum_{i=1}^{N}(x_i - \hat{x}_i)^2 + (y_i - \hat{y}_i)^2}}{\sqrt{N}} \tag{32}$$

2.8. Position delay

It has to be taken under consideration that data analysis, acquisition and use filters with windows produce delay. The windows size influent the delay (33) as well as the time which is need for data acquisition and analysis (34). So, the maximum delay (represented by a travelled distance) which is produced by system related to speed and window size is expressed by the formula (35).

$$\varepsilon_{DW} = \left\lfloor \frac{k}{2} \right\rfloor \cdot v \cdot \Delta t \tag{33}$$

$$\varepsilon_{DP} = v \cdot \Delta t \tag{34}$$

$$\varepsilon_P = \left(\left\lfloor \frac{k}{2} \right\rfloor + 1\right) \cdot v \cdot \Delta t \tag{35}$$

Preprints (www.preprints.org) | NOT PEER-REVIEWED | Posted: 25 October 2018 doi:10.20944/preprints201810.0609.v1

Table 2 presents how maximum delay – ε_P, changes with windows size and speed. Delays increase linearly with window size – **Figure 7**. For real time locating system (RTLS) it will be necessary to use additional subsystem that has high frequency of data acquisition if the delay of using only UWB system is too high. Values about delay and information about movement direction (using e.g. MEMS sensors [7]) can be used for position prediction between the successive position from UWB system.

Table 2. Maximum position delay expressed in the travelled distance by the object.

Window size k	Series					
	R1	R2	R3	R4	R5	R6
1	4.11	8.22	12.33	16.44	20.56	24.67
3	8.22	16.44	24.67	32.89	41.11	49.33
5	12.33	24.67	37.00	49.33	61.67	74.00
7	16.44	32.89	49.33	65.78	82.22	98.67
9	20.56	41.11	61.67	82.22	102.78	123.33
11	24.67	49.33	74.00	98.67	123.33	148.00
13	28.78	57.56	86.33	115.11	143.89	172.67
15	32.89	65.78	98.67	131.56	164.44	197.33

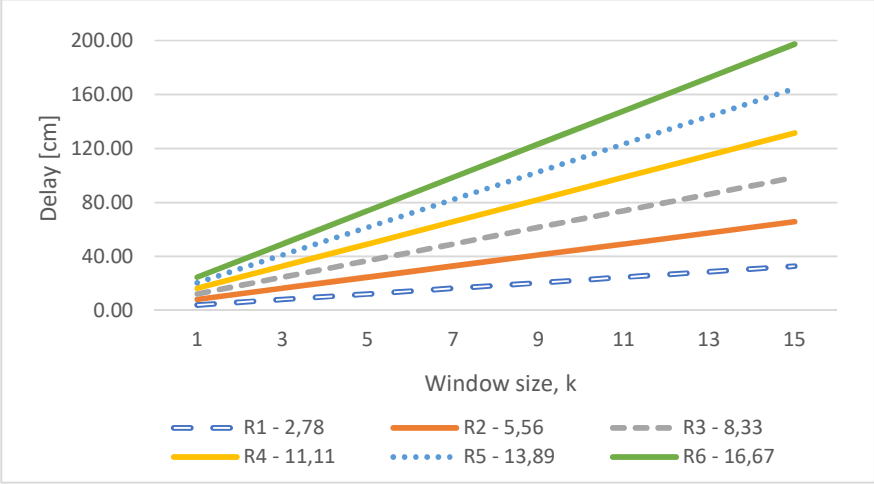

Figure 7. Maximum position delay expressed in the travelled distance by the object.

3. Results and discussion

The mean absolute error of position, maximum deviation, root mean square error and standard error are presented in the Table 2, obtained for raw data and referring to distance were adopted as a reference data for further calculations.

Table 2. Results of statistical measures for raw data.

Statistical measures	Series					
	R1	R2	R3	R4	R5	R6
MAE [cm]	27.59	22.21	19.93	16.21	15.99	13.64
MAX [cm]	75.76	42.06	47.91	39.28	40.95	45.33
RMSE [cm]	30.58	24.05	21.90	18.62	18.17	15.92
SE [cm]	1.70	1.90	1.99	2.03	2.20	2.05

Preprints (www.preprints.org) | NOT PEER-REVIEWED | Posted: 25 October 2018 doi:10.20944/preprints201810.0609.v1

The results deviate significantly from the values declared by the producer (Section 1). Both the placement of antennas in the vehicle and the upward disturbances around it can affect this as well as the speed of the vehicle.

The first suggested methods of data processing were Distance Dependent Error Correction (DDEC) – block B in Section 2.1; and Outliers Removal (OR) – block C and D in Section 2.1. The first of them provided improvement up to 3.32 cm (R2), the second improved the results to 1.08 cm (R3). Their combination gave an improvement up to 4.40 cm (R2).

Table 3. Mean Absolute Error of Position for Outliers Removal, Distance Dependent Error Correction and OR+DDEC.

MAE	Series						
Correction	R1	R2	R3	R4	R5	R6	Average
RAW [cm]	27.59	22.21	19.93	16.21	15.99	13.64	19.26
DDEC [cm]	24.96	18.88	17.48	14.17	14.28	12.66	17.70
OR [cm]	26.97	21.15	18.84	16.15	15.24	13.40	18.62
DDEC + OR [cm]	24.46	17.81	16.23	14.03	13.55	12.43	16.42

The result of the correction was the improvement of the position obtained from 2% - 5% for OR up to even 20% when using DDEC+OR combination. This allowed us to approach the accuracy declared by the manufacturer, when determining the distance from one reference point. It is worth to mention that there is also an error of multilateration process (the average for all series after correction DDEC + OR was 16.42 cm – 2.84cm better than for the RAW data, and only 16.42cm difference from the manufacturer's accuracy for one distance at a speed of up to 5 m/s).

The next stage of the research was to carry out filtration with fundamental filters i.e. median, moving average and Savitzky-Golay filters. The obtained results of the RMSE of distance for the exemplary two series – R1 and R5; are presented respectively on the Figure 8 and Figure 9.

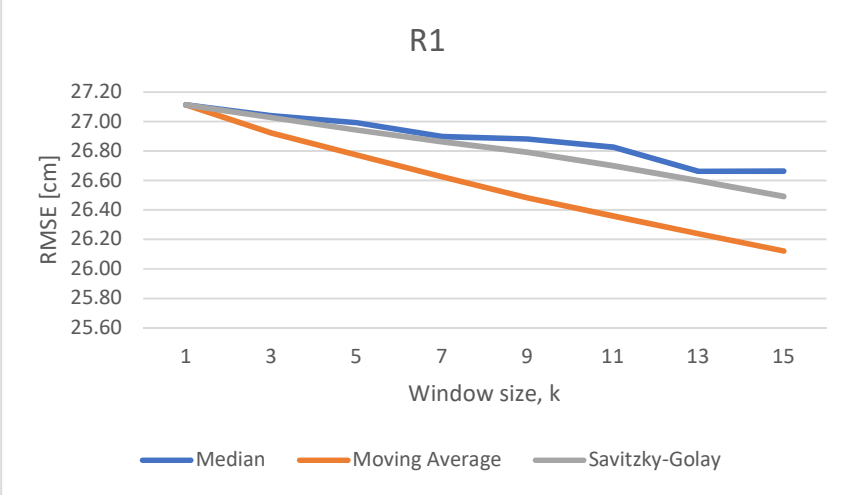

Figure 8. RMSE results for median, moving average and Savitzky-Golay filters for R1 series

The best RMSE results for data filtration with fundamental filters, at the lowest speed are obtained for the moving average filter - the error is 0.99 cm lower. In addition, there is a noticeable improvement in the results obtained with the increase of the filter window size. The other filters obtained a similar result, 0.45 cm for the median filter and 0.62 cm for the Savitzky-Golay. At this speed, using a filter with a moving window of size 15 generates 32,89 cm of delay (what was presented in Section 2.8).

Preprints (www.preprints.org) | NOT PEER-REVIEWED | Posted: 25 October 2018 doi:10.20944/preprints201810.0609.v1

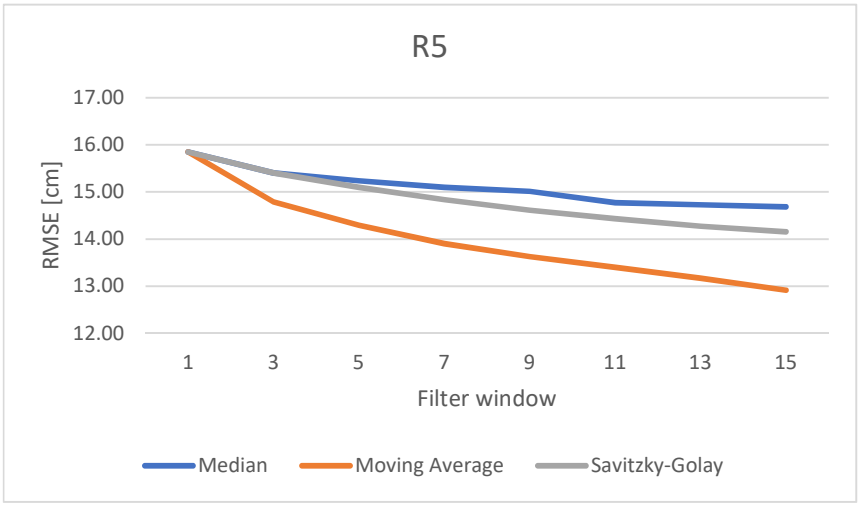

Figure 9. RMSE results for median, moving average and Savitzky-Golay filters for R5 series

In relation to above graph, like in the R1 series, the best RMSE results for data filtration with fundamental filters, at the R5 speed are obtained for the moving average filter – the error is here 2.93 cm lower. The noticeable improvement for median results with the increase in the size of the filter window occurs here to the size of window 3. Later changes are less significant, but they still occur. For moving average filtration, a significant improvement is also visible for the filter window 3. Then the error decreases almost linearly.

Figure 10 presents the results for smoothing process (both DDEC and OR) and filtering process using Kalman and Wiener method separately for each measurement series. Standard error gives an opportunity to compare results which are achieved on unequal number of samples in data set. In average, Kalman filtration gives slightly better results in both cases – with full smoothing process and without it. The percentage error (based on average value for each speed value) for both Kalman and Wiener filtration is approximately 7%. In comparison, Figure 11 presents average RMSE and MAE values across all measurement series (from R1 to R6).

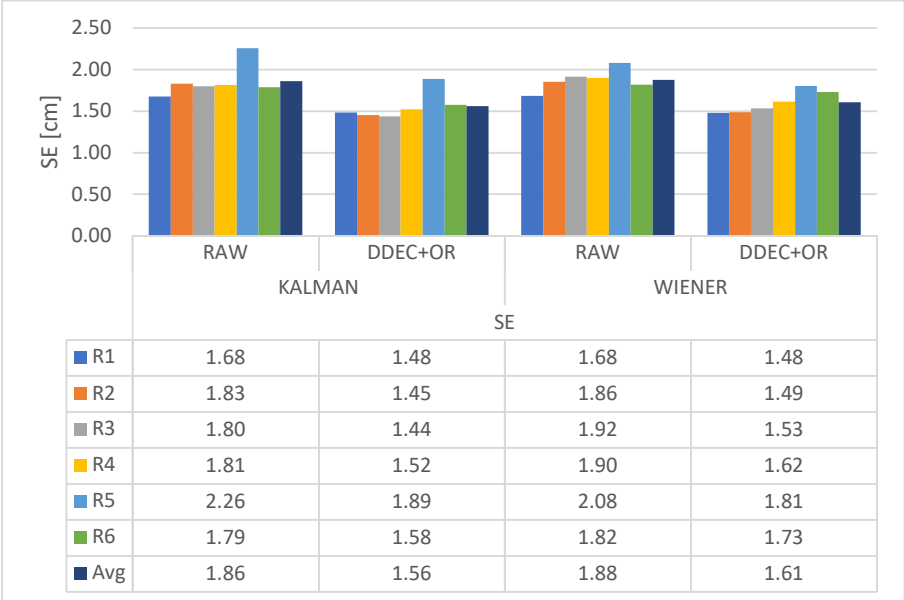

	KALMAN RAW	KALMAN DDEC+OR	WIENER RAW	WIENER DDEC+OR
R1	1.68	1.48	1.68	1.48
R2	1.83	1.45	1.86	1.49
R3	1.80	1.44	1.92	1.53
R4	1.81	1.52	1.90	1.62
R5	2.26	1.89	2.08	1.81
R6	1.79	1.58	1.82	1.73
Avg	1.86	1.56	1.88	1.61

Figure 10. Comparison of Kalman and Wiener filters, for all test series (R1 to R6) using both DDEC+OR smoothing methods and without it

Preprints (www.preprints.org) | NOT PEER-REVIEWED | Posted: 25 October 2018 doi:10.20944/preprints201810.0609.v1

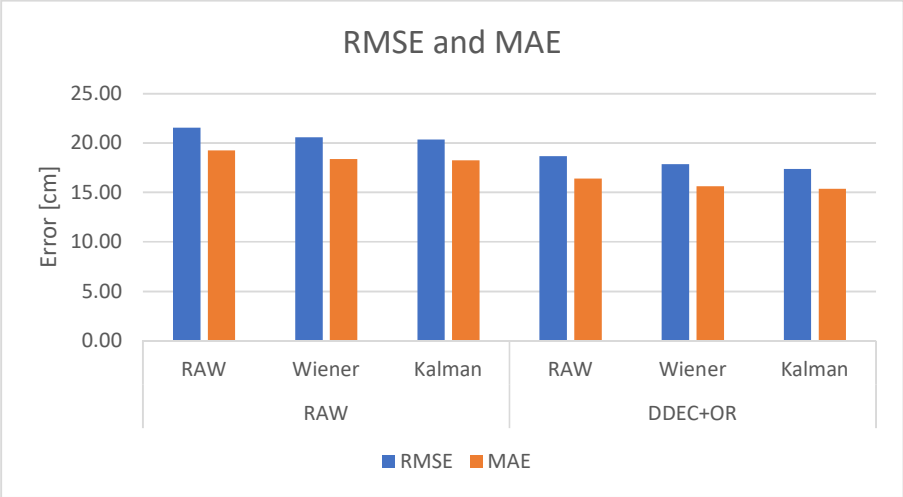

Figure 11. The average value of RMSE an MAE across all measurement series

The final stage was to combine the smoothing process (both DDEC and OR), prefiltration of three different types of filtration – median, mean and Savitzky-Golay; and finally, main filtration using Kalman filter - Figure 12. As we can see, the best results were obtained for the moving average with Kalman filtration for all test series. In addition, the table also shows that the values for R6 has dropped up to 50%. The other filtration methods also improved the results, but only the improvement for the Kalman filter in combination with the moving average pre-filtration is noticeable for all measuring series.

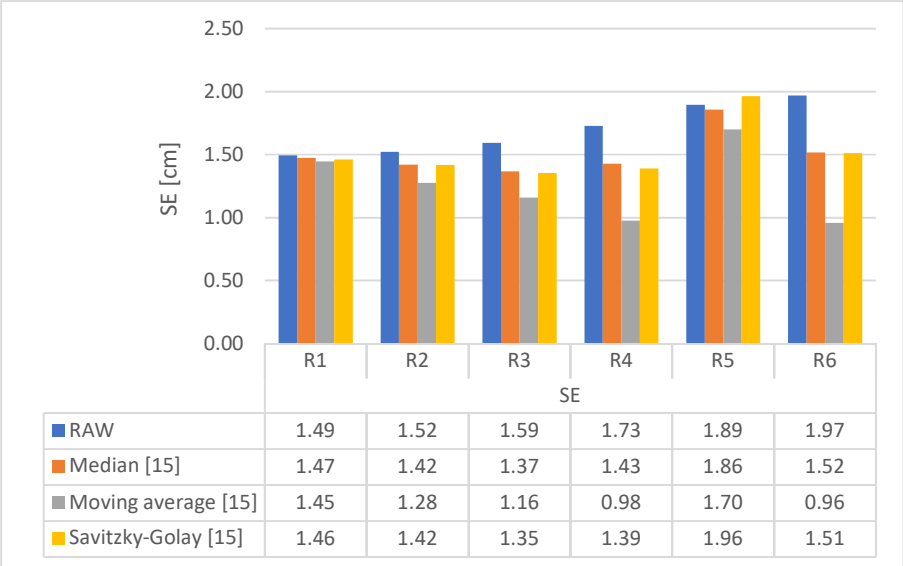

	R1	R2	R3	R4	R5	R6
RAW	1.49	1.52	1.59	1.73	1.89	1.97
Median [15]	1.47	1.42	1.37	1.43	1.86	1.52
Moving average [15]	1.45	1.28	1.16	0.98	1.70	0.96
Savitzky-Golay [15]	1.46	1.42	1.35	1.39	1.96	1.51

Figure 12. Comparison of SE for Kalman filter, with use of median, moving average and Savitzky-Golay – window size 15, as well as DDEC + OR for all test series

For best filtration process – DDEC and OR smoothing process, pre-filtration by moving average and main filtration by Kalman filter, the 10th to 90th percentiles of position error for R4 and R6 are presented respectively on Figure 13 and Figure 14. For R4 series in average about 70% of measurements have error of position lower than half maximum error value. In case of R6 series 90% of measurements have error of position lower than half maximum error value.

Preprints (www.preprints.org) | NOT PEER-REVIEWED | Posted: 25 October 2018 doi:10.20944/preprints201810.0609.v1

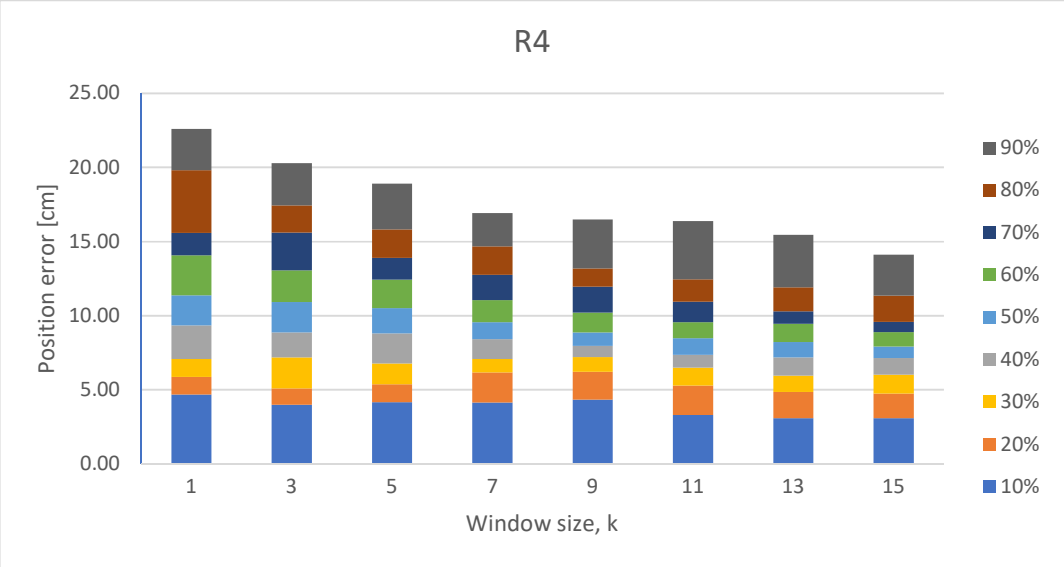

Figure 13. The 10th to 90th percentiles of position error for R4 data series (11.11 m/s)

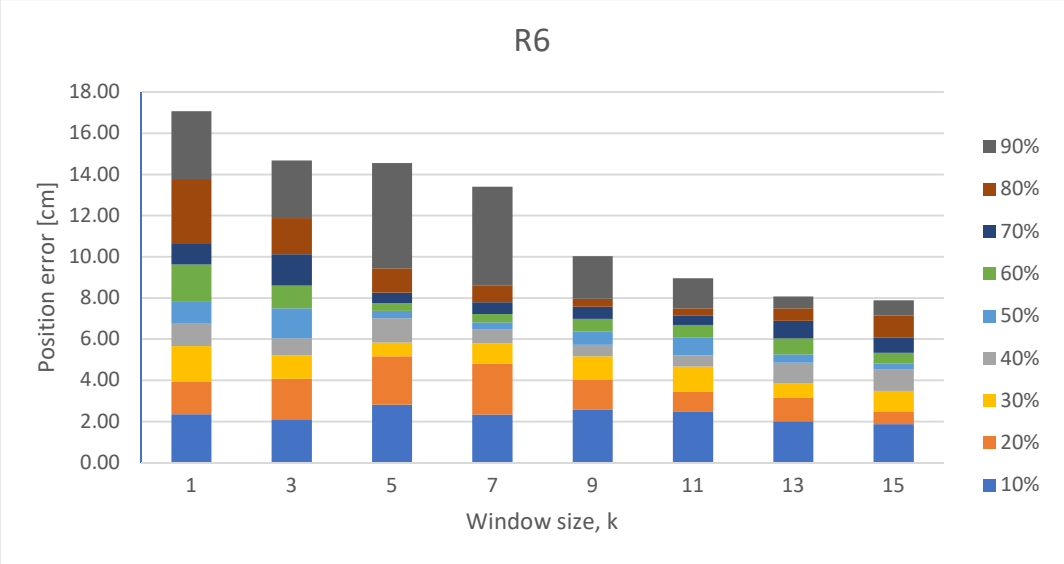

Figure 14. The 10th to 90th percentiles of position error for R6 data series (16.67 m/s)

5. Conclusions

Based on the research, it can be said that there is the possibility of positioning objects in urban traffic (up to 60 km/h) using the UWB system. However, one must keep in mind the existing limitations of this technology e.g. response time is not deterministic.

The results indicate that for vehicle traffic UWB data, they are susceptible to the occurrence of extreme outliers. In addition, it is possible to correct them using a suitably designed function that is based on statistical analysis of acquired samples.

Depending on the metric used, the best results of filtration of data from the UWB system were obtained for the combination of DDEC, OR filtration, Kalman filter and moving average with window 15 for MAE, MAX and RMSE. The best result of the improvement, averaged across all speeds was from 8% (MAX), 17% (MAE, RMSE) up to 20% (SE). Obviously, the important issue is filter window size, e.g. for higher speeds, filters with window 7 and above gave equally good results, which suggests that using a higher window size leads to longer delay with constant accuracy.

Preprints (www.preprints.org) | NOT PEER-REVIEWED | Posted: 25 October 2018 doi:10.20944/preprints201810.0609.v1

The experiments showed that the accuracy declared by the manufacturer of 10 cm is reflected in the raw data error from one reference point and static object. After the trilateration, the cumulative error from the four reference points is larger (RMSE 15.92 cm – 30.58 cm), however, if the filtration is used, even for vehicular traffic in urban conditions (60 km/h), authors are able to obtain the position RMSE accuracy of 7.60 cm – 12.50 cm however the position information delay have to be taken under consideration.

In the case of an RTLS system, it is required to use a high-frequency positioning subsystem. Higher operation of the positioning subsystem guarantees smaller impact of the distance travelled on the total position error resulting from the system error and shift of the moving object.

Thus, the presented solution corresponds to the thesis presented in the assumptions of the study, and its use - considering the precision of operation below 1 meter for high speed - can be widely used in smart city or industry 4.0 applications.

Author Contributions: conceptualization, D.G., K.H. and K.P.; methodology, D.G., K.H. and K.P.; software, K.H. and K.P.; validation, D.G.; formal analysis, K.H. and K.P.; investigation, D.G., K.H., K.P.; data curation, K.H. and K.P.; writing—original draft preparation, K.H. and K.P.; writing—review and editing, D.G.; visualization, K.H. and K.P.; supervision, D.G.; project administration, D.G.; funding acquisition, D.G.

Funding: This work was supported by the Ministry of Science and Higher Education funding for statutory activities.

Conflicts of Interest: The authors declare no conflict of interest. The funders had no role in the design of the study; in the collection, analyses, or interpretation of data; in the writing of the manuscript, or in the decision to publish the results.

References

1. Alarifi, A.; Al-Salman, A.; Alsaleh, M.; Alnafessah, A.; Al-Hadhrami, S.; Al-Ammar, M. A.; Al-Khalifa, H. S. Ultra Wideband Indoor Positioning Technologies: Analysis and Recent Advances. *Sensors (Basel)* **2016**, *16*, doi:10.3390/s16050707.
2. Kamiński, Ł.; Bruniecki, K. Mobile Navigation System for Visually Impaired Users in the Urban Environment. *Metrology and Measurement Systems* **2012**, *19*, 245–256, doi:10.2478/v10178-012-0021-z.
3. Lehtinen, M.; Happonen, A.; Ikonen, J. Accuracy and time to first fix using consumer-grade GPS receivers. In *2008 16th International Conference on Software, Telecommunications and Computer Networks*; 2008; pp. 334–340.
4. Agrawal, M.; Konolige, K. Real-time Localization in Outdoor Environments using Stereo Vision and Inexpensive GPS. In *18th International Conference on Pattern Recognition (ICPR'06)*; 2006; Vol. 3, pp. 1063–1068.
5. Yang, P.; Wu, W.; Moniri, M.; Chibelushi, C. C. Efficient Object Localization Using Sparsely Distributed Passive RFID Tags. *IEEE Transactions on Industrial Electronics* **2013**, *60*, 5914–5924, doi:10.1109/TIE.2012.2230596.
6. Ni, L. M.; Liu, Y.; Lau, Y. C.; Patil, A. P. LANDMARC: Indoor Location Sensing Using Active RFID. *Wireless Networks* **2004**, *10*, 701–710, doi:10.1023/B:WINE.0000044029.06344.dd.
7. Grzechca, D.; Tokarz, K.; Paszek, K.; Poloczek, D. Using MEMS Sensors to Enhance Positioning When the GPS Signal Disappears. In *Computational Collective Intelligence*; Lecture Notes in Computer Science; Springer, Cham, 2017; pp. 260–271.
8. Biswas, J.; Veloso, M. WiFi localization and navigation for autonomous indoor mobile robots. In; IEEE, 2010; pp. 4379–4384.
9. Combain Mobile AB CPS - Combain Positioning Service Available online: https://combain.com (accessed on Jul 8, 2017).

Preprints (www.preprints.org) | NOT PEER-REVIEWED | Posted: 25 October 2018 doi:10.20944/preprints201810.0609.v1

10. Wang, X.; Xu, K.; Li, Z. SmartFix: Indoor Locating Optimization Algorithm for Energy-Constrained Wearable Devices Available online: https://www.hindawi.com/journals/wcmc/2017/8959356/ (accessed on Oct 15, 2017).
11. Constandache, I.; Bao, X.; Azizyan, M.; Choudhury, R. R. Did You See Bob?: Human Localization Using Mobile Phones. In *Proceedings of the Sixteenth Annual International Conference on Mobile Computing and Networking*; MobiCom '10; ACM: New York, NY, USA, 2010; pp. 149–160.
12. Fischer, G.; Dietrich, D.; Winkler, F. Bluetooth indoor localization system 2004.
13. Cantón Paterna, V.; Calveras Augé, A.; Paradells Aspas, J.; Pérez Bullones, M. A. A Bluetooth Low Energy Indoor Positioning System with Channel Diversity, Weighted Trilateration and Kalman Filtering. *Sensors* **2017**, *17*, 2927, doi:10.3390/s17122927.
14. Aalto, L.; Göthlin, N.; Korhonen, J.; Ojala, T. Bluetooth and WAP Push Based Location-aware Mobile Advertising System. In *Proceedings of the 2Nd International Conference on Mobile Systems, Applications, and Services*; MobiSys '04; ACM: New York, NY, USA, 2004; pp. 49–58.
15. Grzechca, D.; Pelczar, P.; Chruszczyk, Ł. Analysis of Object Location Accuracy for iBeacon Technology based on the RSSI Path Loss Model and Fingerprint Map. *International Journal of Electronics and Telecommunications* **2016**, *62*, 371–378.
16. Jin, M.; Fu, C.; Yu, C.; Lai, H. I 3 BM Zigbee Positioning Method for Smart Home Applications. *International Journal of Smart Home* **2008**.
17. Liu, F.; Chen, C.; Kao, Y.; Hong, C.; Yang, C. Improved ZigBee module based on fuzzy model for indoor positioning system. In *2017 International Conference on Applied System Innovation (ICASI)*; 2017; pp. 1331–1334.
18. Israel, A.; Dehy, R. INFRARED TRACKING SYSTEM 2004.
19. Kato, H.; Billinghurst, M. Marker tracking and HMD calibration for a video-based augmented reality conferencing system. In; IEEE Comput. Soc, 1999; pp. 85–94.
20. Bernardin, K.; Stiefelhagen, R. Evaluating Multiple Object Tracking Performance: The CLEAR MOT Metrics. *J Image Video Proc* **2008**, *2008*, 246309, doi:10.1155/2008/246309.
21. Pescaru, D.; Curiac, D.-I. Anchor Node Localization for Wireless Sensor Networks Using Video and Compass Information Fusion. *Sensors* **2014**, *14*, 4211–4224, doi:10.3390/s140304211.
22. Gezici, S.; Tian, Z.; Giannakis, G. B.; Kobayashi, H.; Molisch, A. F.; Poor, H. V.; Sahinoglu, Z. Localization via ultra-wideband radios: a look at positioning aspects for future sensor networks. *IEEE Signal Processing Magazine* **2005**, *22*, 70–84, doi:10.1109/MSP.2005.1458289.
23. Utter, M. *Indoor Positioning using Ultra-wideband Technology*; 2015;
24. Knobloch, D. Practical challenges of particle filter based UWB localization in vehicular environments. In *2017 International Conference on Indoor Positioning and Indoor Navigation (IPIN)*; 2017; pp. 1–5.
25. ScenSor Module DWM1000 - WSN | DecaWave Available online: https://www.decawave.com/products/dwm1000-module;https://web.archive.org/web/20180824023046/https://www.decawave.com/products/dw1000 (accessed on Oct 19, 2017).
26. An Algebraic Solution to the Multilateration Problem (PDF Download Available) Available online: https://www.researchgate.net/publication/275027725_An_Algebraic_Solution_to_the_Multilateration_Problem (accessed on Aug 1, 2017).
27. Premebida, C.; Nunes, U. Segmentation and geometric primitives extraction from 2D laser range data for mobile robot applications. *Robotica* **2005**, *2005*.

Preprints (www.preprints.org) | NOT PEER-REVIEWED | Posted: 25 October 2018 doi:10.20944/preprints201810.0609.v1

28. Breckon, T. *2D Target tracking using Kalman filter*; 2016;
29. Lim, J. S. *Two-dimensional signal and image processing*; Prentice Hall signal processing series; Prentice Hall: Englewood Cliffs, N.J, 1990; ISBN 978-0-13-935322-2.